

One-dimensional variational (1-D Var) retrieval of temperature, water vapor, and a reference pressure from radio occultation measurements: A sensitivity analysis

Axel von Engel¹, Gerald Nedoluha¹, Gottfried Kirchengast², and Stefan Bühler³

Received 3 September 2002; revised 23 January 2003; accepted 26 February 2003; published 5 June 2003.

[1] A 1-D Var retrieval study of simulated radio occultation measurements is presented. Temperature and a water vapor profile are retrieved along with a reference pressure to generate the pressure profile by applying the hydrostatic equation. High-resolution European Center for Medium-Range Weather Forecasts (ECMWF) atmospheric fields are used by a ray tracing tool to calculate the exact positions of the tangent point. The 1-D atmospheric profiles following the calculated tangent point trajectory in the 3-D ECMWF fields are used to simulate bending angle measurements with a 1-D forward model. Assimilation of these bending angles in a 1-D Var tool employing the same 1-D forward model is performed. We analyze the sensitivity of the retrieval to changes in vertical resolution, horizontal smearing of the tangent point trajectory, and the assumption of hydrostatic equilibrium for a nonvertical atmospheric scan. We find that retrievals calculated without adequate vertical resolution can have significant errors in temperature and water vapor. Errors in the retrieval by assuming hydrostatic equilibrium for a nonvertical scan generally cause only minor errors in the retrieved profiles. A study into the occurrence of rays curving down toward the Earth surface indicates that about 5–10% of the profiles could experience so-called critical refraction at altitudes between 0.5 km and 2 km in case of the applied high-resolution ECMWF data. *INDEX TERMS:* 0350 Atmospheric Composition and Structure: Pressure, density, and temperature; 3260 Mathematical Geophysics: Inverse theory; 3360 Meteorology and Atmospheric Dynamics: Remote sensing; *KEYWORDS:* 1DVar, radio occultation, critical refraction, duct, hydrostatic equation

Citation: von Engel, A., G. Nedoluha, G. Kirchengast, and S. Bühler, One-dimensional variational (1-D Var) retrieval of temperature, water vapor, and a reference pressure from radio occultation measurements: A sensitivity analysis, *J. Geophys. Res.*, 108(D11), 4337, doi:10.1029/2002JD002908, 2003.

1. Introduction

[2] Global Navigation Satellite Systems (GNSS), such as the American Global Positioning System (GPS), the Russian Global Navigation Satellite System (GLONASS), or the future European Galileo system, provide a continuous source of signals at radio frequencies. These signals can be used for atmospheric remote sensing. Ground based GNSS receivers can be used to derive information about the integrated precipitable water vapor [Bevis *et al.*, 1992], while airborne or spaceborne receivers are capable of retrieving profile information on temperature and water vapor [Fischbach, 1965; Kursinski *et al.*, 1997; Zuffada *et al.*, 1999]. Combinations of ground based and space-borne

GNSS receivers have also been investigated for simulated tropospheric water vapor imaging [Foelsche and Kirchengast, 2001].

[3] The radio occultation geometry for a spaceborne GNSS receiver in a low Earth orbit (LEO) detecting signals from GNSS satellites is shown in Figure 1. The bending angle α can be expressed as a function of the impact parameter a or the radius to the tangent point r_t , as given in Figure 1. The impact parameter is defined as the distance between the Earth's center and the perpendicular on the asymptotic ray path. The radius to the tangent point is defined as the point along the path closest to the surface of the Earth.

[4] The situation given in Figure 1 holds only for local spherical symmetry. Deviations from local spherical symmetry are introduced by atmospheric inhomogeneities and by the elliptical shape of the Earth. The elliptical shape of the Earth can be compensated for by the introduction of a different Earth's center and a radius of curvature, depending on longitude, latitude, and the position of the occultation plane. This radius is a fit to the actual shape of the Earth at the occultation event, it is larger than the Earth's radius at the poles and smaller than the Earth's radius at the equator.

¹Naval Research Laboratory, Washington, D. C., USA.

²Institute for Geophysics, Astrophysics, and Meteorology, University of Graz, Graz, Austria.

³Institute of Environmental Physics, University of Bremen, Bremen, Germany.

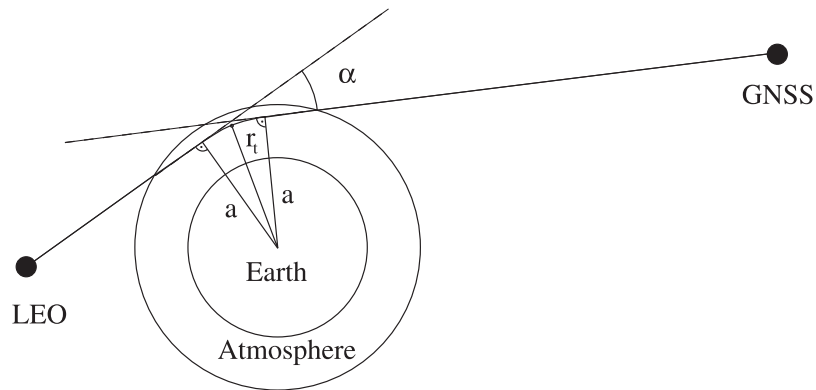


Figure 1. Radio occultation geometry in a spherically symmetric medium, the impact parameter a , the bending angle α , and the radius to the tangent point r_t are indicated.

For a more thorough error discussion, please refer to *Zou et al.* [2002]. The influence of deviations from a spherical symmetric atmosphere cannot be corrected this easily and will in general introduce errors in the retrieved atmospheric profiles, [e.g., *Healy*, 2001a].

[5] A first proof-of-concept mission for radio occultation was the GPS Meteorology (GPS/MET) experiment [*Ware et al.*, 1996]. The instrument was launched in April 1995 onboard the small research satellite MicroLab-1. The mission continued until March 1997, measuring up to 150 GPS setting occultation per day during dedicated periods. The possible 250 setting events per day were not reached, owing to gaps in the ground station network tracking and memory limitations onboard the satellite. In total, about 70 000 occultation events were collected. Several thousand events have been compared with correlative data sets and a statistical agreement within 1 K mean temperature for an altitude range of 1 km to 40 km was found [*Rocken et al.*, 1997].

[6] Most of the early retrievals of temperature and water vapor profiles from radio occultation measurements focused on a direct retrieval approach, thus no a priori (also called first guess, or background) information was incorporated. This allowed for the determination of a dry temperature profile where the amount of water vapor was insignificant. At lower tropospheric altitudes either temperature or water vapor can be determined assuming that the other quantity is known. Recently, several authors have addressed the process of bending angle or refractivity assimilation by variational systems. These systems are defined by the number of dimensions considered and span the range from 1-D Var to 4-D Var, [e.g., *Palmer et al.*, 2000; *Healy and Eyre*, 2000; *Kuo et al.*, 2000; *Liu et al.*, 2001], and allow for the simultaneous determination of temperature and water vapor profiles.

[7] Within this study we shall use simulated radio occultation measurements made from a single LEO satellite for one particular day in 2001 (19 May 2001). This day lies within the time frame of a Naval Research Laboratory assimilation study, focusing on the impact of radio occultation data on a Numerical Weather Prediction (NWP) model. One LEO satellite, using only signals of the GPS constellation, would be able to detect about 250 setting events and 250 rising events per day [*Kursinski et al.*, 1997], a fully installed GLONASS or Galileo system would double the

number of soundings. About 550 GPS occultation events were found for our simulated LEO satellite, and a subset of 110, chosen to provide a wide range of latitude measurements, was used in this study. Measurements were simulated using a ray tracing model and a high-resolution ECMWF data set. A 1-D Var retrieval method was used to derive temperature and water vapor profiles, and a reference pressure. The primary purpose of this study is to provide quantitative assessments of the errors caused by several approximations which are commonly made in retrieving atmospheric parameters from GPS occultation measurements.

[8] Additionally, we investigate the occurrence of so-called critical refraction in this ECMWF data set. Critical refraction occurs when the radius of curvature of the ray is equal to the radius of curvature of the atmosphere, causing the ray to propagate at a fixed height above the surface. Below the critical refraction limit, the ray is bend down toward the Earth surface and the signal might be lost. Critical refraction is currently investigated as one possible factor for a present negative bias in radio occultation refractivity data at low altitudes, as well as a source for corruptions (e.g. signal loss) in the data (G. Hajj et al., CHAMP and SAC-C atmospheric occultation results and intercomparisons, submitted to *Journal of Geophysical Research*, 2002). The corruption and the bias depend on latitude, they are stronger in the tropics than in polar regions [*Sokolovskiy*, 2001].

[9] Our paper is structured as follows: sections 2 and 3 introduce the forward and retrieval model. Section 4 discusses the impact of the retrieval grid upon the generation of the pressure profile. Section 5 discusses the impact of fine-scale structure in the temperature and water vapor profiles upon the retrieval capabilities. Section 6 discusses the influence of the reference pressure retrieval altitude. Sections 7 and 8 discuss horizontal displacement of the tangent point and the associated deviation from hydrostatic conditions. Section 9 gives possible improvements in the a priori profiles. Section 10 discusses occurrence of critical refraction. Finally, section 11 gives the conclusion.

2. Forward Model Setup

[10] Two forward models have been used in this study, a 3-D ray tracing tool, and a 1-D forward model. Within the

3-D ray tracing tool, ECMWF atmospheric analysis fields of 19 May 2001 with 4 time steps, 60 vertical levels, and a T511 horizontal resolution were used [Miller, 1999; Teixeira, 1999; Jakob et al., 2000]. The vertical resolution of these fields gradually increases from 20 m at the surface to about 250 m at 1 km altitude, and about 1 km to 3 km in the stratosphere. The horizontal resolution is about 0.351° . The upper limit of these fields is around 65 km. We use the MSIS atmosphere for altitudes above 65 km [Hedin, 1987, 1991].

[11] In this study we calculate bending angles using a 1-D forward model, with the temperature and water vapor values taken from ECMWF values at the tangent point locations calculated by the 3-D ray tracer. The range of temperatures and water vapor values should therefore serve as a representative sample of values which will be measured on a daily basis by a single LEO satellite. We shall focus on the effects of a high vertical resolution atmospheric field on a 1-D forward calculation and a 1-D assimilation process. Since a 1-D assimilation process will be quick and efficient, it is anticipated that operational assimilation of radio occultation measurements will incorporate a 1-D approach.

2.1. Three-Dimensional Ray Tracer

[12] The End-to-end GNSS Occultation Performance Simulator (EGOPS [Kirchengast, 1998; Kirchengast et al., 2002]) tool was used to derive the actual location of the tangent points in the 3-D ECMWF fields. EGOPS reads in orbital parameters for the GNSS and the LEO satellites and predicts in a first step the approximate occultation locations. The actual occultation locations are determined by the positions of the satellites and the influence of the atmosphere on the ray. Within this first step, the atmospheric influence is approximated by a simple bi-exponential atmospheric model consisting of a dry component (bulk atmosphere) and a wet component (water vapor distribution). Both dry air density and water vapor density are assumed to decrease exponentially with height based on a constant scale height [Kirchengast, 1998].

[13] In the second step, EGOPS reads in atmospheric fields and uses a ray tracer with sub-millimeter accuracy to calculate the actual ray path and the precise occultation location. The ray tracer terminates when one of the rays hits the Earth's surface, thus not all occultations reach down to the surface. Almost all 110 simulated occultations reach tangent altitudes ≤ 5 km, but only about 30 reach tangent altitudes < 1 km.

[14] The ray tracing procedure includes ionospheric effects simulated by a 3-D ionosphere with a solar activity index of 130 (10.7 cm flux). Additional features of the EGOPS software allow for the simulation of the complete measurement chain, including receiver effects, to calculate bending angles. As mentioned above, the EGOPS bending angles are not used in this study. This allows us to simplify the forward calculation and to avoid the introduction of additional errors caused by ionospheric effects, receiver effects, or discrepancies between the two forward models.

2.2. One-Dimensional Forward Model

[15] The forward model used in this study is 1-dimensional, and therefore neglects the effects of horizontal variations in the atmosphere. It has already been used for

a combination study of a radio occultation with a passive microwave instrument [von Engel et al., 2001].

[16] The principle equations of the radio occultation 1-D forward model are given by Kursinski et al. [1997]; the calculation of the bending angle α as a function of refractivity follows an Abelian integral equation, refractivity itself depends on pressure, temperature, and water vapor.

[17] The forward Abel integral is given by:

$$\alpha(a) = 2a \int_{r=r_t}^{r=\infty} \frac{1}{\sqrt{(nr)^2 - a_t^2}} \frac{d \ln(n)}{dr} dr \quad (1)$$

where the integration is performed through all altitudes r down to the tangent point r_t , and the factor 2 results from the assumed symmetric atmosphere. The refractive index is given by n and the impact parameter at r_t is $a_t = nr_t$. The internal resolution for the evaluation of equation (1) in the 1-D forward model is set to 0.05 km to capture the high-resolution ECMWF fields. Input profiles are cubic-spline fitted to this resolution.

[18] Table 1 summarizes the α error and the sampling (reflecting the resolution) of the measurement. Bending angles are transformed from the internal forward resolution to the given resolution by averaging over the corresponding vertical intervals. Fresnel diffraction will generally lead to a resolution of about 0.5 km in the lower atmosphere, but a strong vertical refraction gradient can contribute to an improved resolution of up to 100 m for very strong gradients [Kursinski et al., 1997]. Thus a measurement resolution of 250 m assures that altitude regions with strong gradients are in general adequately covered. We assumed reasonable error characteristics which are in-between the "proof-of-concept" GPS/MET instrument and expected accuracies of modern receivers [European Space Agency, 1998]. Measurement errors were assumed to be unbiased (i.e., systematic errors are negligible), since this observation technique is self-calibrating. Useful determination of α above 60 km is not possible, due to the poor signal-to-noise ratio of mesospheric radio occultation data.

[19] The 1-D model neglects horizontal variations in the atmosphere. The impact of horizontal variations has been addressed in several publications, [e.g., Palmer et al., 2000; Healy, 2001a; Ahmad and Tyler, 1999; Foelsche and Kirchengast, 2002]. The limb path through the atmosphere leads to a very coarse horizontal resolution on the order of 200 km, thus the observed radio occultation signal is effectively averaged over this horizontal interval. Syndergaard et al. [2002] have shown that, in cases where the horizontal gradient is large, it is possible to significantly improve the accuracy of the retrieval by mapping the two-dimensional structure into a one-dimensional profile. Because such a mapping procedure provides a one-dimensional approximation to three-dimensional atmosphere, all of the results presented here are relevant to such an approximation.

2.3. Diffraction Effects

[20] Neither ray tracing nor Abel integral based forward models consider explicitly the effects of Fresnel diffraction, which will limit the vertical resolution of the measurement to approximately the diameter of the first Fresnel zone (if no diffraction correction is performed). The size of the first

Table 1. Sampling Grid Used for the Simulated Measurements Along With the Corresponding Bending Angle Errors Assumed

Height, km	Sampling dz , km	Error, μrad
$00 \leq z \leq 25$	0.25	4.0
$25 \leq z \leq 40$	0.50	2.8
$40 \leq z \leq 60$	1.00	2.0

Fresnel Zone is usually around 0.5 km in the lower atmosphere, and increases to more than 1 km in the upper stratosphere [Kursinski *et al.*, 1997]. The internal processing of the 1-D forward model used to calculate bending angles at the resolution given in Table 1 results in variations in vertical resolution which are similar to those caused by Fresnel smoothing.

3. Retrieval Model

[21] The inverse model I calculates the most likely solution $\hat{\mathbf{x}}$ of the atmospheric state \mathbf{x} . An iterative approach is necessary because the retrieval of temperature and water vapor profiles from radio occultation measurements can be nonlinear. The retrieval algorithm used here is based on the 1-D Var or Optimal Estimation Method [Rodgers, 2000]. It uses a priori knowledge on the state of the atmosphere to stabilize the solution.

[22] The iterative formula to calculate $\hat{\mathbf{x}}$ for the iteration $n + 1$ is given as:

$$\hat{\mathbf{x}}_{n+1} = \mathbf{x}_0 + \mathbf{G}_n[(\mathbf{y} - \mathbf{y}_n) - \mathbf{K}_n(\mathbf{x}_0 - \hat{\mathbf{x}}_n)] \quad (2)$$

where \mathbf{x}_0 is the a priori vector from which the iteration starts, \mathbf{G}_n the n th iteration of the gain matrix, \mathbf{y} represents the bending angle measurement, \mathbf{y}_n the forward model output, and \mathbf{K}_n the Jacobian.

[23] The Jacobian matrices \mathbf{K}_n and \mathbf{G}_n are defined as:

$$\mathbf{K}_n \equiv \left. \frac{\partial F(\mathbf{x})}{\partial \mathbf{x}} \right|_{\mathbf{x}=\mathbf{x}_n} \quad \mathbf{G}_n \equiv \left. \frac{\partial I(\mathbf{y})}{\partial \mathbf{y}} \right|_{\mathbf{y}=\mathbf{y}_n=F(\mathbf{x}_n)} \quad (3)$$

where $F(\mathbf{x})$ is the forward model discussed in the previous section, which creates simulated measurements for any given state \mathbf{x} .

[24] For this study the Jacobian matrix \mathbf{K}_n is calculated by perturbing the corresponding retrieval parameter \mathbf{x} of $F(\mathbf{x})$. For the given formulation the matrix \mathbf{G}_n can be calculated from:

$$\mathbf{G}_n = \left(\mathbf{S}_0^{-1} + \mathbf{K}_n^T \mathbf{S}_y^{-1} \mathbf{K}_n \right)^{-1} \mathbf{K}_n^T \mathbf{S}_y^{-1} \quad (4)$$

with the a priori error covariance matrix \mathbf{S}_0 , the error covariance matrix of the measurement \mathbf{S}_y , and \mathbf{K}_n^T denoting the transpose matrix of \mathbf{K}_n .

[25] The 1-D Var allows the calculation of two statistical errors, each of which contributes to the total error of the retrieval. Generally one can write the total retrieval error covariance matrix \mathbf{S} as:

$$\mathbf{S} = \mathbf{S}_S + \mathbf{S}_M \quad (5)$$

where \mathbf{S}_S is the smoothing error covariance matrix, and \mathbf{S}_M is the measurement error covariance matrix. Furthermore, one defines the averaging kernel matrix \mathbf{A} as:

$$\mathbf{A} = \mathbf{GK} \quad (6)$$

Making use of this notation the individual error matrices can be calculated as:

$$\mathbf{S}_S = (\mathbf{A} - \mathbf{I})\mathbf{S}_0(\mathbf{A} - \mathbf{I})^T \quad (7)$$

$$\mathbf{S}_M = \mathbf{G}\mathbf{S}_y\mathbf{G}^T \quad (8)$$

where \mathbf{I} denotes the identity matrix. It is assumed within this study that \mathbf{S}_0 in equation (7) is identical to the a priori knowledge \mathbf{S}_0 in equation (4).

[26] The smoothing error represents the error in those portions of profile space where the observing system is insensitive. This includes, for example, small scale variations that cannot be detected due to the limited altitude resolution [Rodgers, 2000]. The measurement error is due to noise in the measured bending angles that has propagated into the retrieval.

[27] We shall assume that the measurement error covariance and the a priori error covariance are statistical in nature (i.e., the measurement profile and the a priori profile have no systematic bias). This assumption is generally fulfilled for the bending angle measurement [Rieder and Kirchengast, 2001] but is often not true for the a priori profile. Generally, the a priori profiles and its error covariance matrices have to be chosen very carefully for a retrieval from real data, in order to avoid the introduction of a bias [Rodgers, 2000].

3.1. Retrieval Setup

[28] The $\hat{\mathbf{x}}$ vector holds in this investigation the temperature profile between 0 km and 100 km, the water vapor profile between 0 km and 20 km, and a reference pressure from which the hydrostatic atmospheric pressure profile is generated. The reference pressure is usually retrieved at the lowest retrieval altitude. The vertical retrieval grid is given in Table 2. The vertical resolution of radio occultation is limited by Fresnel smoothing which imposes a resolution limit of about 0.5 km, so we have chosen a retrieval grid with approximately this resolution. Retrieval of temperature with a 1 km resolution is feasible up to 40 km, at higher altitudes the signal-to-noise ratio limits the retrieval capabilities. Retrieval above 60 km is not possible with the chosen setup, nevertheless the extension of the temperature grid up to altitudes of 100 km assures that uncertainties in the mesospheric temperatures will be considered in the error budget at lower altitudes. Contributions to the error budget arise from the limb sounding geometry.

[29] The \mathbf{S}_0 matrix is generated with a 2.5 K a priori uncertainty for temperatures up to 20 km and a linear increase up to 20 K at 100 km. For water vapor a 40% uncertainty is assumed, and a 1% error in the reference pressure. The measurement covariance matrix \mathbf{S}_y is generated with the errors presented in Table 1. A conservative approach for correlations (off-diagonal elements) in \mathbf{S}_0 and \mathbf{S}_y was taken, where both matrices are assumed to be diagonal. For a more thorough discussion on the effect of correlations on the retrieval products, please refer to Healy [2001b].

[30] A NWP model short range forecast calculation can provide an a priori temperature and water vapor profile. The forecast uncertainty for temperature of an NWP model is

Table 2. Vertical Retrieval Grid

Species	Height, km	Sampling dz , km
Temperature	$00 \leq z \leq 30$	0.5
Temperature	$30 \leq z \leq 40$	1.0
Temperature	$40 \leq z \leq 60$	2.5
Temperature	$70 \leq z \leq 100$	10.0
Water Vapor	$00 \leq z \leq 20$	0.5

about 2.0 K for the lower atmospheric layers (up to 20 km) and increases to about 15 K at 65 km [Palmer *et al.*, 2000]. Water vapor forecast is possible with an uncertainty of about 40% [Palmer *et al.*, 2000]. Hence our a priori profile uncertainties reflect current forecast capabilities of NWP models. The 1% a priori uncertainty for the reference pressure retrieval is a conservative assumption, but sensitivity of the retrieval to this uncertainty is very low.

4. Influence of the Retrieval Grid on the Pressure Profile

[31] A pressure profile is required for the calculation of the bending angles. The $\hat{\mathbf{x}}$ vector holds one reference pressure, usually at the lowest retrieval altitude. The pressure profile is generated by integrating the hydrostatic equation over the retrieval grid.

[32] The hydrostatic equation is given by:

$$p_i = p_{i-1} / \exp(\Delta\Phi \cdot g_a / (R_d \cdot \bar{T}_v)) \quad (9)$$

where p_i is the pressure at retrieval level i , p_{i-1} the pressure at the retrieval level below, $\Delta\Phi$ the difference in geopotential between level i and $i+1$, g_a the standard acceleration of gravity (9.80665 m/s^2), R_d the gas constant for dry air (287.06 J/kg/K), and \bar{T}_v the mean virtual temperature between the layers i and $i+1$. Using the virtual temperature instead of the actual temperature makes it possible to use the gas constant for dry air R_d instead of the gas constant for moist air, which would depend on the humidity content [Salby, 1996]. It is calculated at each retrieval level as:

$$T_v = T \cdot (1.0 + 0.608 \cdot q) \quad (10)$$

where T is the temperature and q the specific humidity (mass of water vapor per unit mass of dry air) in [g/g] at that level. Rewriting equation (9) allows a downward integration.

[33] The accuracy of the hydrostatic equation integration depends on the resolution of the retrieval grid, since \bar{T}_v in equation (9) is approximated by the mean virtual temperature at the retrieval levels i and $i+1$ which in turn depends on the temperature and water vapor at these levels. Figure 2 (top) shows the errors in the pressure and bending angle profiles for occultation number 100 (Location: 69.2°S , 25.0°E) resulting from the use of different vertical retrieval grids. Shown are the deviations of a lower resolution pressure profile with respect to a profile calculated on a higher vertical resolution that covers all variability in the ECMWF fields. All pressure profiles were calculated following equation (9) with a pressure initialization at the surface. The temperature and water vapor profiles of the lower resolutions are averaged over the corresponding area

of the high-resolution profile, since a lower resolution in the retrieval process will average over that high-resolution interval. The lower resolution profiles are then interpolated back to the high-resolution grid for comparison, using an exponential interpolation.

[34] Deviations in pressure or bending angle from the high-vertical resolution pressure profile will only occur for resolutions coarser than the resolution of the underlying ECMWF fields, which is better than 0.5 km for the lower atmosphere and typically around 1 to 2 km for the upper atmosphere. The deviations shown are typical for all profiles, deviations in pressure for the lower atmosphere are generally below 1% for a 2 km vertical resolution grid, and above 1% for a 5 km vertical resolution grid. The retrieval grid resolution as given in Table 2 does not introduce significant pressure errors in the lower atmosphere where the radio occultation method is sensitive.

[35] On the right hand side of Figure 2 (top) the error in the bending angles is shown, where bending angles have been calculated on the grid defined in Table 1, using the different vertical resolution profiles. Errors are calculated with respect to bending angles derived from the high-vertical resolution profiles. The errors are complicated by the fact that they do not only depend on pressure, but more strongly on temperature and water vapor than the hydrostatic equation. Thus altitude regions where the temperature and/or water vapor profile has a lot of fine-scale structure that is smoothed with the applied retrieval resolution will show deviations from the high-resolution bending angle calculation. Consequently the resulting errors in bending angle are much more complicated. Errors larger than 10% for the 2 km and 5 km resolutions can be found for certain occultations. Bending angle errors introduced by the chosen retrieval grid are negligible at altitudes between 5 km and 40 km but can reach more than 5% for some occultations at altitudes near the surface where the ECMWF fields have a resolution better than 0.1 km. Bending angle errors introduced by the chosen retrieval grid at altitudes above 55 km can reach several percent, but the retrieval sensitivity at these altitudes is very low, where signal-to-noise ratios near unity occur. Retrievals from improved receivers with lower noise would benefit from the use of a higher-resolution grid in the mesosphere.

5. Influence of Fine-Scale Structures in the Temperature and Water Vapor Profiles on the Retrieval

[36] To assess the error of these fine-scale structures in the temperature and water vapor profile, 1-D Var retrieval calculations were performed for the 110 occultations observed by our simulated LEO satellite. The measurement vector was generated with the high-resolution ECMWF atmosphere fields. The a priori was calculated from the high-resolution fields by averaging it over the corresponding retrieval resolution, thus this scenario presents a retrieval calculation where the a priori is set as closely as possible to the true profile. For this investigation, all occultation locations were extrapolated down to the lowest possible retrieval altitude, given either by the surface orography or the lowest altitude that showed no critical refraction (see section 10). The corresponding latitude and

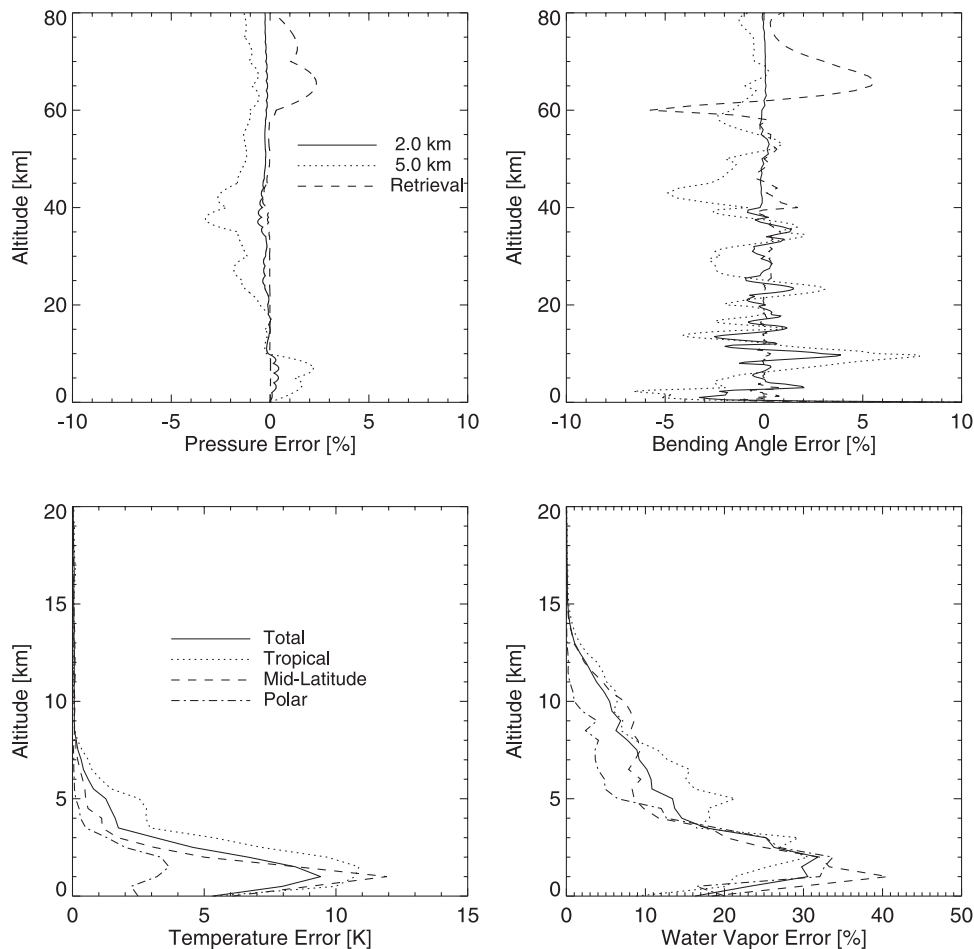


Figure 2. (top) Errors in pressure (left) and resulting errors in bending angles (right) for occultation 100 caused by different equidistant vertical grids and the chosen retrieval grid as given in Table 2. (bottom) Mean absolute error of the retrieved profiles caused by fine-scale structures in the bending angle measurements, (right) temperature and (left) water vapor.

longitude of the occultation were found by linearly extrapolating the longitude and latitude positions found in the ray tracing process over the altitude grid, thus approximating the horizontal displacement of the tangent point. The following calculations are all made using the reference pressure altitude at the lowest possible retrieval altitude, with a hydrostatic atmosphere assumed above this altitude.

[37] Figure 2 (bottom) shows the mean of the absolute difference between the true profiles and the retrieved profiles, where the difference is calculated for each occultation and retrieval level. This error has been separated into latitude bands to investigate the influence of particular geographical regions. The mean latitude θ of an occultation defines the latitude band as: tropical $|\theta| < 30^\circ$, polar $|\theta| > 60^\circ$, and midlatitudes in between. The total number of occultations falling into a specific band is: tropical 45, midlatitude 38, polar 27.

[38] As is shown in Figure 2 (bottom), uncharacterized fine-scale structure in the atmosphere can lead to severe errors in the retrieval. Especially affected are tropical and midlatitude occultations, where temperature errors larger than 10 K are observed, and water vapor errors can reach more than 30%. In this simulation the errors occur only at the lower altitudes, where the ECMWF fields have a very

fine resolution to capture the highly variable lower troposphere. The retrieval is unable to follow these small-scale variations and starts to oscillate around the true solution. These large errors almost completely disappear if one uses a higher retrieval resolution of 0.25 km in the lower troposphere. Maximum errors in temperature, water vapor of about 0.1 K, 5% respectively, are found with this setting. The maximum errors in water vapor occur at lower altitudes, where the ECMWF fields have a sufficient resolution to capture the highly variable water vapor profile. A separation into different latitude bands shows that the errors in temperature are almost independent of latitude. Water vapor errors are more than twice as high in polar regions (about 10%), compared to tropical and midlatitude ones (about 4%).

[39] Hence for retrieval from bending angle measurements one must either integrate the bending angles to the retrieval grid, or use a retrieval grid that captures the fine-scale structures in the troposphere. It is possible that ambiguous results found by *Palmer and Barnett* [2001] were caused by these fine-scale structures. The assimilation of refractivity measurements should not be affected as strongly as the bending angle measurements, since the vertical correlations are higher and the assimilation process

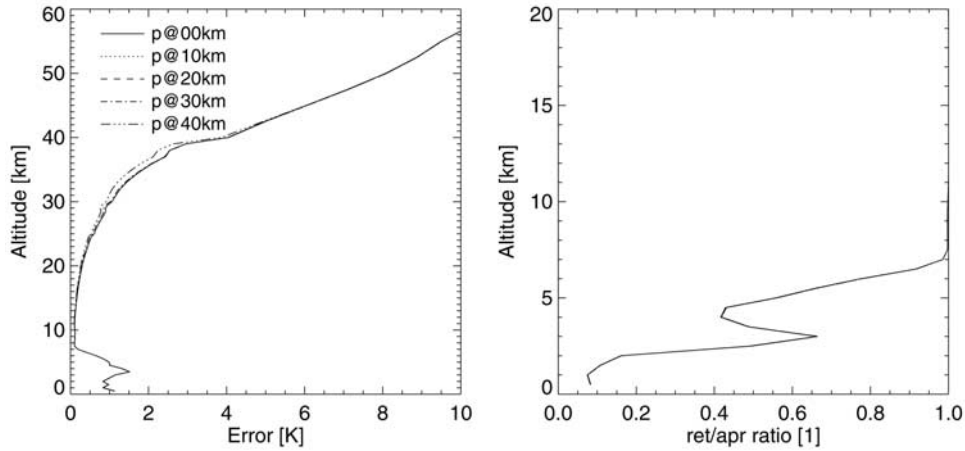


Figure 3. Retrieval error for temperature (left) and water vapor error ratios ϵ (right) for occultation 245 for different altitudes of the reference pressure retrieval.

does not require the calculation of a second derivative, as is necessary for the pole-free version of equation (1).

6. Altitude of the Reference Pressure Retrieval

[40] The hydrostatic equation as given by equation (9) can be integrated upward or downward, and the specific altitude chosen for the reference pressure retrieval changes the retrieval accuracy for temperature or water vapor only marginally. Figure 3 shows the retrieval error of the temperature and the error ratio of the water vapor retrieval for a representative midlatitude occultation (Occultation 245, Location: 40.8°S, 56.4°W). Different reference pressure retrieval altitudes are evaluated, starting near the surface and extending up to 40 km. Error ratios ϵ which provide a measure of the sensitivity of the retrieval to the observation, are calculated at each retrieval level i for water vapor as:

$$\epsilon = \sqrt{S[i, i]} / \sqrt{S_0[i, i]} \quad (11)$$

Note that an error ratio of 1 indicates that all the information is provided by the a priori. Total retrieval errors, as provided by the diagonal elements of \mathbf{S} are shown for temperature.

[41] As can be seen in Figure 3, a very small improvement in the temperature profile retrieval is observed for a reference pressure retrieval at higher altitudes. The water vapor retrieval accuracy is not affected. The feature in all error ratio profiles at about 3 km is caused by a strong water vapor gradient around this altitude.

7. Horizontal Displacement of the Tangent Point

[42] The latitude and longitude of the tangent point will generally change during an occultation event both because of the motion of the satellites and because of the variation of atmospheric refractivity with altitude. This horizontal displacement is, at high altitudes, mainly caused by changes in the occultation geometry, while at lower altitudes the atmospheric contribution dominates.

[43] Figure 4 (left) shows the average horizontal displacement for all occultations and separated by latitude bands starting at a tangent altitude of 60 km. The geometric contribution varies linearly with altitude, and is about 80 km at the surface. The total horizontal displacement is

around 200 km, with higher values found for tropical conditions, and lower ones for polar conditions. Figure 4 (left) underestimates the average horizontal displacement at lower altitudes since, just as for observations, occultations in regions with low refractivity variations are more likely to reach lower altitudes in the ray tracing model, while strong variations will more often lead to a termination of the ray tracing process higher up in the atmosphere because rays may be bent downward and hit the Earth's surface.

[44] The zenith angle, defined as the angle between the zenith and the tangent point trajectory at each tangent altitude, is shown in Figure 4 (right). As already mentioned in connection with the horizontal displacement, the zenith angles at higher altitudes are determined by the geometry of the observation. Polar occultations show lower zenith angles because the GPS orbit inclination is about 55° thus all observations are made toward the South or North. All occultations reach zenith angles around 85° independent of the latitude band at low altitudes.

8. Deviations From a Hydrostatic Atmosphere

[45] The ECMWF fields are hydrostatic in the vertical, but due to the horizontal displacement of the tangent point discussed above, the resulting pressure profile along the tangent point trajectory might deviate from the hydrostatic approximation.

[46] To investigate the error introduced by assuming a hydrostatic atmosphere for GPS occultation measurements, we first calculated a hydrostatic pressure profile using the 1-D temperature and water vapor profiles at the tangent point locations in the 3-D ECMWF fields. This hydrostatic pressure profile calculation was initialized with the pressure value found in the 3-D ECMWF fields at 60 km. The hydrostatic pressure profile was then compared with the actual pressure at the tangent point locations in the 3-D ECMWF fields. The percentage deviation of a pressure profile p_H calculated following the hydrostatic approximation from the actual pressure profile along the tangent point trajectory p_{3-D} was calculated at each altitude level as:

$$\left(\frac{\Delta p_H}{p} \right) = |(p_H - p_{3-D}) / p_{3-D}| \quad [\%] \quad (12)$$

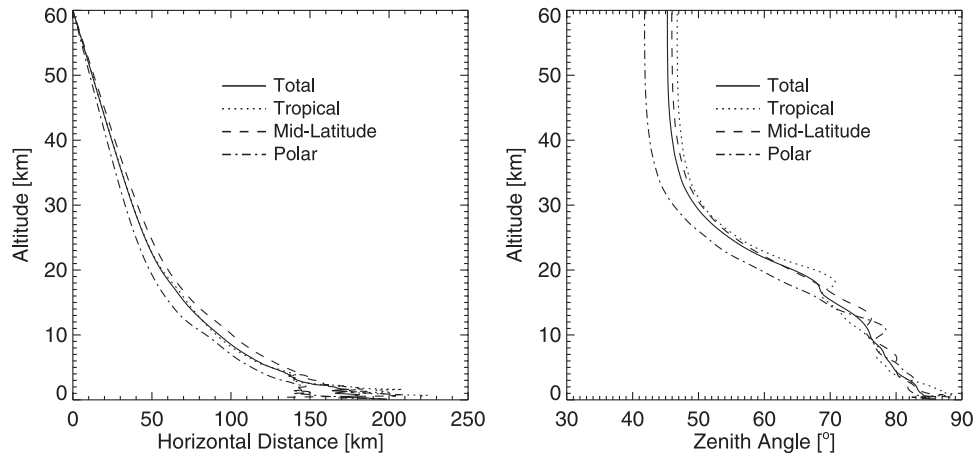


Figure 4. Averaged horizontal displacement of tangent point (left) and zenith angle (right), total and for different latitude bands. Noise has been removed from the zenith angle calculations by boxcar (also called sliding window) averaging data over 1 km intervals.

[47] Figure 5 shows the mean of $\left(\frac{\Delta p_H}{p}\right)$ for all occultations and separated by latitude bands. The mean of $\left(\frac{\Delta p_H}{p}\right)$ over all occultation gradually increases with decreasing altitude and reaches a maximum of about 0.25% near the surface. Minor deviations from the hydrostatic assumption appear for tropical conditions, with a mean of $\left(\frac{\Delta p_H}{p}\right)$ around 0.05%. Occultations occurring at midlatitudes experience larger deviations from a hydrostatic atmosphere, averaging more than 0.4% near the surface. Deviations increase especially in the troposphere where strong temperature and water vapor gradients exist.

[48] The maximum pressure deviation $\max\left(\frac{\Delta p_H}{p}\right)$ was calculated and sorted by value and occultation location to get a more quantitative picture. Table 3 lists the number of occultations falling within various $\max\left(\frac{\Delta p_H}{p}\right)$ intervals.

[49] Out of the 110 occultations processed, most show only minor deviations from a hydrostatic atmosphere. Nevertheless there are a significant number of occultations (about 5%) where pressure deviations of more than 1% from the hydrostatic atmosphere appear. The maximum deviation

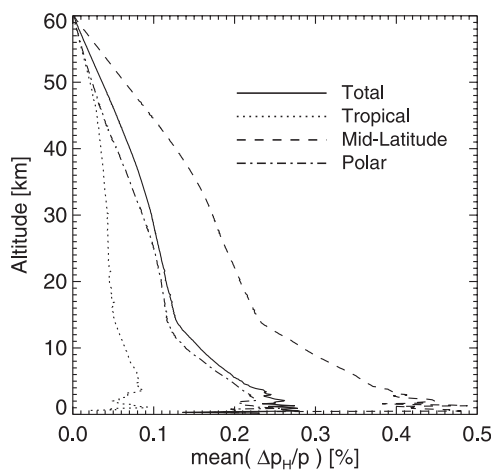


Figure 5. Mean deviation $\left(\frac{\Delta p_H}{p}\right)$ from a hydrostatic pressure profile, total and for different latitude bands.

is around 1.5%. Generally $\left(\frac{\Delta p_H}{p}\right)$ increases almost linearly with distance from the initialization point at 60 km.

[50] The separation by latitude bands shows that tropical and polar occultations generally experience a pressure profile close to hydrostatic, while most of the severe deviations from hydrostatic appear at midlatitudes.

[51] The effect of such a non hydrostatic deviation on the temperature and water vapor retrieval is shown in Figure 6 for two different occultations. Figure 6 (top) shows occultation 100 which experienced a moderate deviation $\max\left(\frac{\Delta p_H}{p}\right)$ from a hydrostatic atmosphere of about 0.4%. The bottom plot shows occultation 245, where a deviation $\max\left(\frac{\Delta p_H}{p}\right) = 1.5\%$ was found. Both retrievals were calculated down to the lowest possible retrieval altitude as given by the surface topography.

[52] Both retrieval calculations were initialized with an a priori profile equal to the true profile (the influence of small-scale features as discussed above have been removed). Hence the difference between the a priori profile and the true profile is zero in Figures 6 (top) and Figures 6 (bottom). Different altitudes for the pressure retrieval were evaluated, where the true pressure value found in the pressure profile p_{3-D} was used as a priori.

[53] Moderate deviations from a hydrostatic atmosphere do not affect the retrieval capabilities significantly (see Figure 6, top). The error introduced in the retrieved temper-

Table 3. Maximum Deviations $\max\left(\frac{\Delta p_H}{p}\right)$ From a Hydrostatic Atmosphere Found Over Atmospheric Pressure Profile

Deviation, %	Total Number of Occultations	Latitude Band		
		Tropical	Midlatitude	Polar
$0.0 \geq \max\left(\frac{\Delta p_H}{p}\right) < 0.1$	36	28	3	5
$0.1 \geq \max\left(\frac{\Delta p_H}{p}\right) < 0.2$	30	12	9	9
$0.2 \geq \max\left(\frac{\Delta p_H}{p}\right) < 0.3$	17	3	9	5
$0.3 \geq \max\left(\frac{\Delta p_H}{p}\right) < 0.4$	9	2	3	4
$0.4 \geq \max\left(\frac{\Delta p_H}{p}\right) < 0.5$	3	0	3	0
$0.5 \geq \max\left(\frac{\Delta p_H}{p}\right) < 0.6$	5	0	2	3
$0.6 \geq \max\left(\frac{\Delta p_H}{p}\right) < 0.7$	2	0	2	0
$0.7 \geq \max\left(\frac{\Delta p_H}{p}\right) < 0.8$	3	0	3	0
$0.8 \geq \max\left(\frac{\Delta p_H}{p}\right) < 0.9$	0	0	0	0
$0.9 \geq \max\left(\frac{\Delta p_H}{p}\right) < 1.0$	0	0	0	0
$\max\left(\frac{\Delta p_H}{p}\right) \geq 1.0$	5	0	4	1

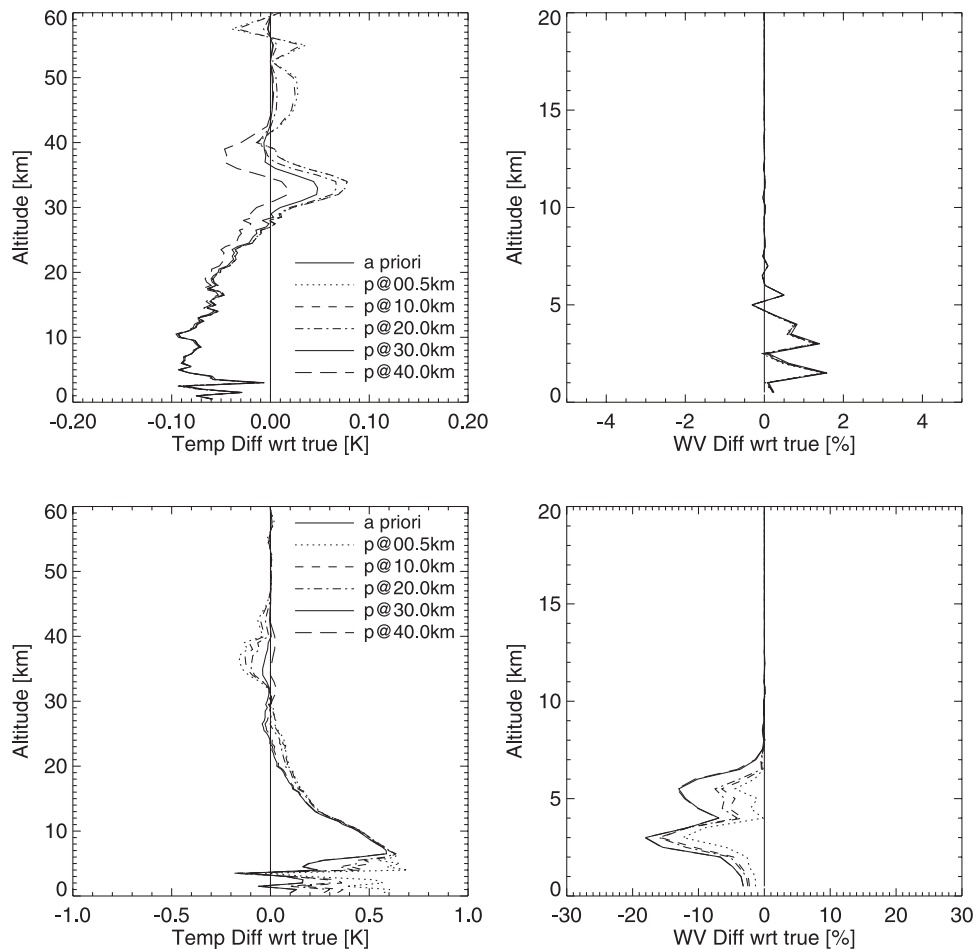


Figure 6. Deviations from the true temperature (left) and water vapor (right) profile for a moderate nonhydrostatic atmosphere (Occultation 100, Location: 69.2°S, 25.0°W, top) and for a severe nonhydrostatic atmosphere (Occultation 245, Location 40.8°S, 56.4°W, bottom).

ature and water vapor profile is very small, with a maximum error of about 0.1 K for temperature, and about 1.5% for water vapor. The retrieval errors show only a minor dependence on the altitude chosen for the pressure retrieval. Only areas with a low signal-to-noise ratio are affected in temperature by the altitude of the reference pressure retrieval. Lowering the altitude of the reference pressure retrieval causes the maximum of the hydrostatic deviation to higher altitudes, since the effect generally increases with distance from the reference altitude. Raising the altitude of the reference pressure retrieval will reduce the hydrostatic deviation at higher altitudes, but will increase the deviation at levels below the reference pressure. Hence the maximum deviations at high altitudes are found for the 0.5 km and 10.0 km reference altitudes. Reference pressure retrievals at higher altitudes will move the effect to lower and higher altitudes.

[54] Larger deviations from a hydrostatic atmosphere lead to more significant errors in the retrieval (see Figure 6, bottom). Maximum temperature errors of about 0.5 K are found for any of the reference pressure altitudes used in this study. Temperature deviations at the lowest altitudes are particularly sensitive to the choice of the reference pressure altitude, since in this region the retrieval is sensitive to both temperature and water vapor. Above about 8 km, where the

influence of water vapor is negligible, the deviations for all reference pressures look very similar, as was shown above. The maximum error in water vapor reaches about 20% for this occultation, where this is mainly caused by the strong water vapor gradient present around 3 km. Other occultations with similar deviations from a hydrostatic atmosphere exhibit errors of <10% in water vapor. Note that we discuss the difference with respect to the true profile. The error ratios, as plotted in Figure 3, are nearly insensitive to the altitude of the reference pressure.

[55] The error in the retrieved reference pressure is about 0.03% for the moderate case, and severe cases can lead to errors of almost 0.5%. The smallest error is generally found for a reference altitude of 20 km and increases with distance from this reference altitude, since the 20 km reference altitude equally distributes the hydrostatic deviations to lower and higher altitudes.

9. Possible Improvements in the First Guess Profiles

[56] Investigations of the 1-D Var retrieval methods, as for example performed by *Palmer et al.* [2000], used a short range model forecast at the mean latitude and longitude location of the occultation to provide the a priori, thus

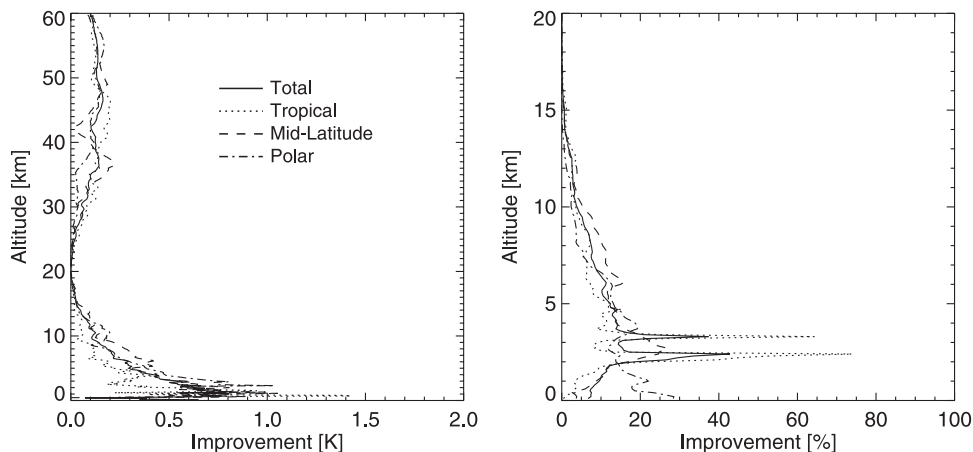


Figure 7. Mean improvement of the temperature (left) and water vapor (right) a priori profile using estimated tangent point locations over a vertical profile taken at a tangent point location corresponding to 20 km tangent altitude, total and for different latitude bands.

ignoring the horizontal displacement of the tangent point. Using an a priori which best approximates the actual temperature and water vapor at the tangent point is especially important in regions where both terms contribute significantly to the refractivity. The EGOPS tool provides the actual 3-D tangent point movement during the ray tracing process. It additionally estimates the horizontal displacement based on the geometry of the occultation and a simple bi-exponential atmosphere. These estimated tangent point trajectories can be used to improve the a priori data.

[57] The improvement I in temperature at each altitude for each occultation is calculated as:

$$I = \text{abs}(T_{true} - T_{mean}) - \text{abs}(T_{true} - T_{est}) \quad (13)$$

with the true temperature profile following the tangent point trajectory in the ECMWF fields T_{true} , the temperature at the estimated tangent point trajectory in the ECMWF fields T_{est} , and the vertical temperature profile in the ECMWF fields at the latitude and longitude of the 20 km tangent altitude T_{mean} . The calculation for water vapor results is similar except that the improvement is expressed in [%].

[58] Figure 7 shows the mean improvement averaged over all occultations. The largest improvements in temperature are found at the lowest altitudes, reaching on average about 0.7 K. No clear latitudinal dependence is visible, but midlatitude occultations show generally slightly larger improvements at the lower altitudes than tropical ones. The corresponding results for the water vapor a priori are shown on the right hand side. Improvements in the water vapor a priori of about 20% are possible at lower altitudes. Improvements tend to decrease at altitudes below 2 km because only a few ray tracing calculations penetrate this low into the atmosphere, and these occultations preferentially encounter only small horizontal gradients in temperature and water vapor. Generally, midlatitude occultations again show a slightly higher possible improvement than tropical occultations. However, there was one tropical occultation, in a situation with strong horizontal gradients, where the improvement was dramatic. This case shows up

as two sharp spikes in Figure 7. This serves to emphasize that there are cases when this effect can be very important.

[59] Results shown in Figure 7 present a best case scenario for 2 reasons: Firstly, the mean improvement is calculated using the true 3-D atmospheric fields, and secondly, the exact tangent point position at 20 km tangent altitude is used. In reality one would use a short term forecast to obtain a priori information, and use the mean and estimated tangent point position within that a priori field. Results obtained from an a priori field are identical to those presented in Figure 7 if: Firstly, the a priori field is very similar to the true field, and secondly, the estimated mean tangent point location is very close to the exact one.

[60] Retrieval calculations, using an ECMWF short term forecast as a priori, were performed for all 110 occultations to determine the possible benefit for 1-D Var retrievals from radio occultation data. Figure 8 (top) shows the errors of the temperature and water vapor retrieval using an a priori at an estimated mean tangent point location. Figure 8 (bottom) shows the same results if one uses the estimated tangent point locations instead. Errors are shown as the mean of the absolute difference to the true profile, where the difference is calculated for each occultation and retrieval level.

[61] The estimated tangent point positions lowered the a priori errors for temperature by about 0.3 K to 0.4 K, and generally by about 5% for water vapor at the lower altitudes. One of the spikes visible in Figure 7 at about 2 km is still visible when using an ECMWF short term forecast and a mean tangent point location. The spike almost disappears in the estimated tangent point positions and here the a priori is improved by about 70%.

[62] Temperature retrieval have improved for all altitudes up to 6 km by about 0.1 K to 0.3 K, above improvements are minor. Water vapor results have improved by a few percent in general for the lower 5 km, and by about 20% at the spike. An ambiguous picture is found above about 6 km tangent altitude. Here, the use of the estimated tangent point locations actually results in a slight degradation of the accuracy of the retrieved profile. This degradation over a small altitude range is a statistical effect caused by the limited size of our data set. In general, however, improving

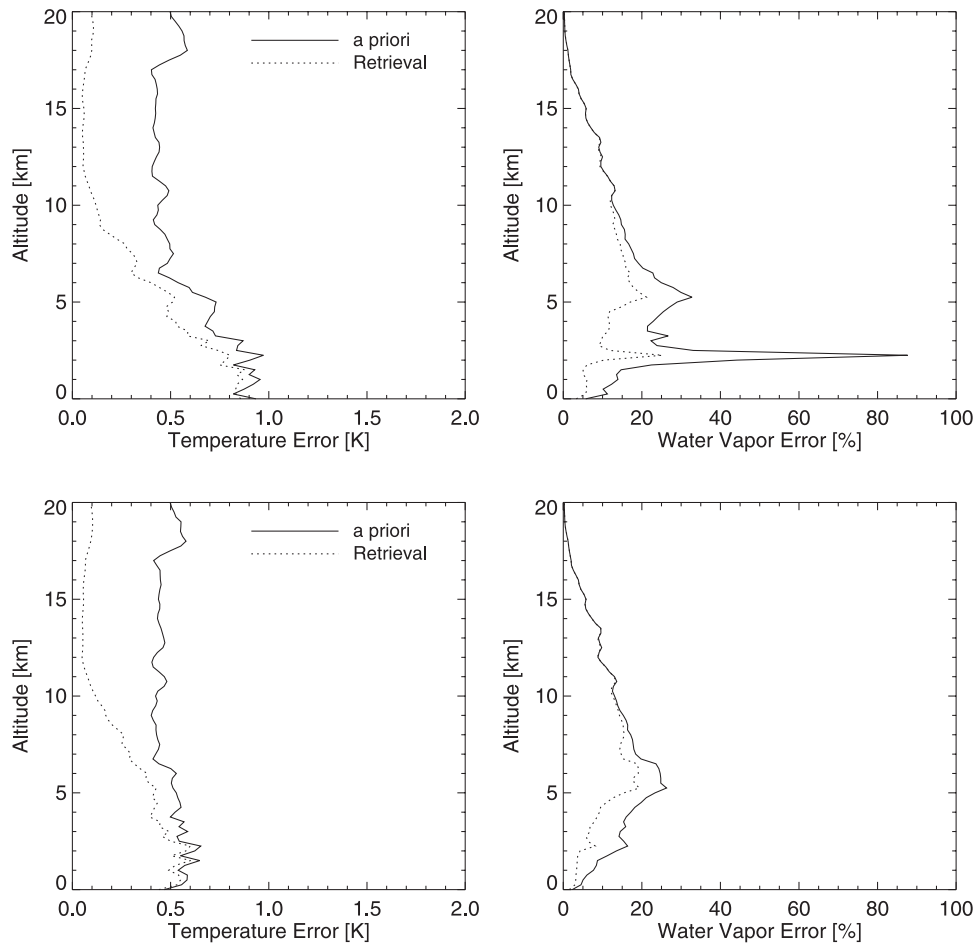


Figure 8. Mean absolute errors of temperature and water vapor profile retrieval using an ECMWF short term forecast a priori. (top) A priori at mean tangent point location. (bottom) A priori following estimated tangent point positions.

the estimate of the atmosphere at the actual tangent point improves the a priori estimate of the atmosphere, and hence improves the retrieval results.

10. Critical Refraction

[63] Conditions for critical refraction are reached when the refractivity gradient dN/dr is about -157 N-units/km. Such large negative refractivity gradients are usually associated with a large vertical gradients of water vapor in the lower troposphere [Kursinski *et al.*, 1997]. Refractivity gradients < -157 N-units/km are associated with super refraction, a condition under which the ray is bent down toward the surface of the Earth.

[64] Since the EGOPS ray tracing algorithm terminates the calculation as soon as one of the rays intersects the surface, which frequently occurs above 2 km, the latitude and longitude position of occultation events which terminated higher in the atmosphere were linearly extrapolated to the lowest possible altitude as given by the surface orography. The refractivity and the gradient are calculated on the internal 1-D forward model grid.

[65] Figure 9 displays the minimum refractivity gradient found for almost all of the 110 simulated occultation events used in this study. The occultations where the minimum in

the refractivity gradient was found above this interval did not show conditions for critical refraction.

[66] Out of the 110 occultations included in this study, 7 occultations show values below the critical refraction limit, mostly for tropical conditions. Fresnel smoothing, as discussed in section 2.3, will push some of the occultations above the threshold, but especially occultations with very low gradients and/or occultations that extend over a range similar to the range over which Fresnel smoothing occurs will still exhibit critical refraction.

11. Conclusions

[67] We have presented a 1-D Var sensitivity analysis of radio occultation measurements using 110 occultations based upon the simulated orbit of a single LEO satellite orbit. A 3-D ray tracing tool together with global high-resolution ECMWF fields was used to derive the actual tangent points of the limb occultation. The ECMWF atmospheric profiles following the tangent point position is used in a 1-D forward and 1-D Var assimilation tool to investigate the effect of high vertical resolution atmospheric fields upon the assimilation of radio occultation data. Atmospheric temperature, water vapor, and a reference pressure for the generation of a hydrostatic pressure profile

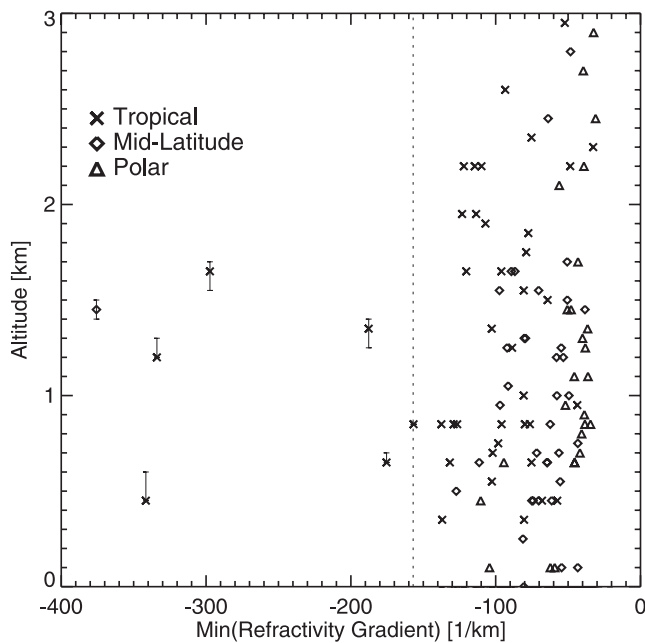


Figure 9. Minimum refractivity gradient along with the associated altitude for all 110 occultations. The vertical bar gives the range over which the gradient is below the threshold for critical refraction. The dotted line marks the limit for critical refraction.

are retrieved. The reference pressure was generally retrieved at the lowest retrieval altitude.

[68] The pressure profile within the 1-D Var assimilation tool is generated by employing the hydrostatic equation. A coarse vertical retrieval grid will introduce errors in the calculated pressure profile since the hydrostatic integration of the pressure profile depends on the temperature and water vapor profiles, and a too coarse profile will integrate over fine-scale structures.

[69] The vertical retrieval resolution of the radio occultation method is limited to about 0.5 km in the troposphere due to Fresnel diffraction and about 1 km in the stratosphere up to 40 km. Above 40 km the signal-to-noise ratio limits the retrieval capabilities. A comparison of the pressure profile calculated on this retrieval grid with a pressure profile calculated on a high-resolution vertical grid shows negligible differences up to 40 km altitude. Equidistant vertical resolutions of 2 km and 5 km show differences below 1% and above 1% respectively.

[70] The errors introduced by the vertical retrieval grid on the bending angles are complicated by the fact that bending angles depend more strongly on the temperature and water vapor profile. Hence fine-scale structure in these profiles can lead to severe errors in the calculated bending angles. A comparison between bending angles calculated on a high vertical resolution grid and on the retrieval grid shows large differences at altitudes below 5 km where a lot of fine-scale structure in the ECMWF data exists. Differences at higher altitudes are generally negligible. Vertical resolutions of 2 km and 5 km can introduce bending angle errors larger than 5% at all altitudes.

[71] Retrieval calculations for all occultations were performed to assess the impact of these fine-scale structures on

the retrieval. The measurements entering the 1-D Var tool were generated with the 1-D forward tool and the high-resolution ECMWF data. The 1-D forward tool was also used in the 1-D Var tool to avoid the introduction of errors caused by different programs. The setup was such that the a priori profile was equal to the profile used in the generation of the measurement averaged onto the coarser retrieval grid, hence the differences could be attributed entirely to inability of the coarser retrieval grid to retrieve fine-scale structures.

[72] At lower altitudes the retrieval of both temperature and water vapor is severely affected by these fine-scale structures. Errors in the temperature retrieval can reach more than 10 K for tropical and midlatitude atmospheric conditions, while errors in the water vapor retrieval can reach more than 30%, almost independent of the atmospheric conditions. A higher vertical resolution in the retrieval removes these severe errors, where temperature and water vapor errors of about 0.1 K and 5% respectively, are found. Thus the retrieval from bending angle measurements requires either a vertical resolution that adequately represents the fine-scale structure in the troposphere, or the integration of bending angles to the coarse resolution used in the retrieval.

[73] The reference pressure retrieval was always performed at the lowest retrieval altitude, an investigation into the effect of the actual reference pressure retrieval altitude showed only minor influence on the retrieval capabilities.

[74] Radio occultation does not provide a vertical scan through the atmosphere. The horizontal displacement of the tangent point in the radio occultation limb scanning measurement is usually around 200 km if one initializes the scan at an altitude of 60 km. About 80 km are due to the geometry, the rest is due to atmospheric refraction. The zenith angle of the tangent point trajectory associated with a vertical scan would be 0° , but is found to be around 45° at altitudes around 60 km and increases to close to 90° at low altitudes.

[75] The atmosphere along the tangent point trajectory deviates from hydrostatic conditions due to the horizontal displacement. Deviations in pressure usually reach a maximum of about 0.2%, but can reach values higher than 1% for certain midlatitude and polar conditions. The effect upon the temperature and water vapor retrieval capabilities is usually negligible but can be important under certain conditions.

[76] It is possible to not only use a mean tangent point location for the determination of the a priori, but to advance to a full tangent point trajectory estimate based on a simple bi-exponential atmosphere. Given ideal a priori data, this improve the a priori of temperature at lower altitudes on average by up to 0.7 K, and the one of water vapor by about 20%. More realistic improvements, using a priori estimates based on a forecast model, result in around 0.3 K reductions in the temperature retrieval error at lower altitudes. Improvements in the retrieval error of about 3% were found at lower altitudes for water vapor.

[77] A preliminary study into critical refraction showed that about 5% of the profiles could be affected. All affected occultations were within or very close to the tropical band at an altitude between 0.5 km and 2 km. The vertical extend over which the signal is lost can be up to about 0.2 km.

[78] **Acknowledgments.** This work was supported by an Internal Government Study from the Integrated Program Office of the National

Polar-orbiting Operational Environmental Satellite System (NPOESS) and by the Office of Naval Research (ONR). The authors wish to thank Dr. N. Kreitz (ECMWF, Reading, UK) and Drs. M. Weber, J. Meyer-Arnek (Institute of Environmental Physics, University of Bremen, Germany) for support with the ECMWF data extraction, Dr. U. Foelsche and Dr. J. Ramsauer (Institute for Geophysics, Astrophysics, and Meteorology, University of Graz, Austria) for help with the EGOPS tool, P. Mills (Naval Research Laboratory, Washington D.C., USA) for support with the IDL programming language, and G. Klowski (SDRK, Walsrode, Germany).

References

- Ahmad, B., and G. Tyler, Systematic errors in atmospheric profiles obtained from Abelian inversion of radio occultation data: Effects of large-scale horizontal gradients, *J. Geophys. Res.*, *104*, 3971–3992, 1999.
- Bevis, M., S. Businger, T. Herring, C. Rocken, R. Anthes, and R. Ware, GPS meteorology: Remote sensing of atmospheric water vapor using the Global Positioning System, *J. Geophys. Res.*, *97*, 15,787–15,801, 1992.
- European Space Agency, The GRAS instrument on METOP, *ESA Rep. VR/3021/PI, EUM Rep. EPS/MIS/IN/9*, 38 pp., Noordwijk, Netherlands, 1998.
- Fischbach, F., A satellite method for temperature and pressure below 24 km, *Bull. Am. Meteorol. Soc.*, *9*, 528–532, 1965.
- Foelsche, U., and G. Kirchengast, Tropospheric water vapor imaging by combination of ground-based and spaceborne GNSS sounding data, *J. Geophys. Res.*, *106*, 27,221–27,231, 2001.
- Foelsche, U., and G. Kirchengast, Sensitivity of atmospheric profiles retrieved from GNSS occultation data to horizontal variability in the troposphere, *Tech. Rep. ESA/ESTEC-2/2002*, 56 pp., Inst. for Geophys., Astrophys., and Meteorol., Univ. of Graz, Graz, Austria, 2002.
- Healy, S., Radio occultation bending angle and impact parameter errors caused by horizontal refractive index gradients in the troposphere: A simulation study, *J. Geophys. Res.*, *106*, 11,875–11,889, 2001a.
- Healy, S., Smoothing radio occultation bending angles above 40 km, *Ann. Geophys.*, *19*, 459–468, 2001b.
- Healy, S., and J. Eyre, Retrieving temperature, water vapour and surface pressure information from a refractive-index profiles derived by radio occultation: A simulation study, *Q. J. R. Meteorol. Soc.*, *126*, 1661–1683, 2000.
- Hedin, A., MSIS-86 thermosphere model, *J. Geophys. Res.*, *92*, 4649–4662, 1987.
- Hedin, A., Extension of the MSIS thermosphere model into the middle and lower atmosphere, *J. Geophys. Res.*, *96*, 1159–1172, 1991.
- Jakob, C., et al., The IFS cycle CY21R4 made operational in October 1999, *ECMWF Newsl.*, *87*, 2–9, 2000.
- Kirchengast, G., End-to-end GNSS Occultation Performance Simulator (EGOPS) overview and exemplary applications, *Wissenschaftl. Ber. 2/1998*, 138 pp., Inst. for Meteorol. and Geophys., Univ. of Graz, Graz, Austria, 1998.
- Kirchengast, G., J. Fritzer, and J. Ramsauer, End-to-end GNSS occultation performance simulator version 4 (EGOPS4) software user manual, *Tech. Rep. ESA/ESTEC-3/2002*, 472 pp., Inst. for Geophys., Astrophys., and Meteorol., Univ. of Graz, Graz, Austria, 2002.
- Kuo, Y., S. Sokolovskiy, R. Anthes, and V. Vandenberghe, Assimilation of GPS radio occultation data for numerical weather prediction, *Terr. Atmos. Oceanic Sci.*, *11*, 157–186, 2000.
- Kursinski, E., G. Hajj, J. Schofield, R. Linfield, and K. Hardy, Observing Earth's atmosphere with radio occultation measurements using GPS, *J. Geophys. Res.*, *102*, 23,429–23,465, 1997.
- Liu, H., X. Zou, H. Shao, R. Anthes, J. Chang, J. Tseng, and B. Wang, Impact of 837 GPS/MET bending angles on assimilation and forecasts for the period June 20–30, 1995, *J. Geophys. Res.*, *106*, 31,771–31,786, 2001.
- Miller, M., Resolution studies, *ECMWF Tech. Memo. 299*, Eur., Cent. for Medium-Range Weather Forecasts, Reading, UK, 1999.
- Palmer, P., and J. Barnett, Application of an optimal estimation inverse method to GPS/MET bending angle observations, *J. Geophys. Res.*, *106*, 17,147–17,160, 2001.
- Palmer, P., J. Barnett, J. Eyre, and S. Healy, A non-linear optimal estimation inverse method for radio occultation measurements of temperature, humidity, and surface pressure, *J. Geophys. Res.*, *105*, 17,513–17,526, 2000.
- Rieder, M., and G. Kirchengast, Error analysis and characterization of atmospheric profiles retrieved from GNSS occultation data, *J. Geophys. Res.*, *106*, 31,755–31,770, 2001.
- Rocken, C., et al., Analysis and validation of GPS/MET data in the neutral atmosphere, *J. Geophys. Res.*, *102*, 29,849–29,866, 1997.
- Rodgers, C., *Inverse Methods for Atmospheric Sounding: Theory and Practice*, *Atmos. Oceanic Planet. Phys. Ser.*, vol. 2, World Sci., River, Edge, N. J., 2000.
- Salby, M., *Fundamentals of Atmospheric Physics, Int. Geophys. Ser.*, vol. 61, Academic, San Diego, Calif., 1996.
- Sokolovskiy, S., Modeling and inverting radio occultation signals in the moist troposphere, *Radio Sci.*, *36*, 441–458, 2001.
- Syndergaard, S., D. Flittner, R. Kursinski, and B. Herman, Simulating the influence of horizontal gradients on refractivity profiles from radio occultation measurements—A promising approach for data assimilation, paper presented at COSMIC Radio Occultation Science Workshop, Univ. Corp. for Atmos. Res., Boulder, Colo, 2002.
- Teixeira, J., The impact of increased boundary layer vertical resolution on the ECMWF forecast system, *ECMWF Tech. Memo. 268*, 55 pp., Eur. Cent. Medium-Range Weather Forecasts, Reading, UK, 1999.
- von Engeln, A., S. Bühler, G. Kirchengast, and K. Künzi, Temperature profile retrieval from surface to mesopause by combining GNSS radio occultation and passive microwave limb sounder data, *Geophys. Res. Lett.*, *28*, 775–778, 2001.
- Ware, R., et al., GPS sounding of the atmosphere from Low Earth Orbit: Preliminary results, *Bull. Am. Meteorol. Soc.*, *77*, 19–40, 1996.
- Zou, X., H. Liu, and R. Anthes, A statistical estimate of errors in the calculation of radio-occultation bending angles caused by a 2D approximation of ray tracing and the assumption of spherical symmetry of the atmosphere, *J. Atmos. Oceanic Technol.*, *19*, 51–64, 2002.
- Zuffada, C., G. Hajj, and E. Kursinski, A novel approach to atmospheric profiling with a mountain-based or airborne GPS receiver, *J. Geophys. Res.*, *104*, 24,435–24,447, 1999.

S. Bühler, University of Bremen, Institute of Environmental Physics, Otto-Hahn-Allee, D-28359 Bremen, Germany. (sbuehler@uni-bremen.de)

G. Kirchengast, University of Graz, Institute for Geophysics, Astrophysics, and Meteorology, Universitätsplatz 5, A-8010 Graz, Austria. (gottfried.kirchengast@uni-graz.at)

G. Nedoluha, Naval Research Laboratory, Code 7227, 4555 Overlook Avenue, SW, Washington, DC 20375 USA. (nedoluha@nrl.navy.mil)

A. von Engeln, Naval Research Laboratory, Marine Meteorology Division, 7 Grace Hopper Avenue, STOP 2, Monterey, CA 93943–5502, USA. (engeln@uni-bremen.de)